RESEARCH ARTICLE
PLANETARY SCIENCES

Earth and Planetary Physics
7: 347–355, 2023
doi: 10.26464/epp2023035

Estimation of surface water content at the Tianwen-1 Zhurong landing site

Xiang Zhou[1,2], Yang Liu[1,3*], Xing Wu[1], ZhenXing Zhao[1,2], and YongLiao Zou[1]

[1]State Key Laboratory of Space Weather, National Space Science Center, Chinese Academy of Sciences, Beijing 100190, China;

[2]University of Chinese Academy of Science, Beijing 100049, China;

[3]Center for Excellence in Comparative Planetology, Chinese Academy of Sciences, Hefei 200083, China

Key Points:

- Atmospheric and thermal corrections were performed on Observatoire pour la Minéralogie, l'Eau, les Glaces et l'Activité (OMEGA) hyperspectral data covering the Zhurong landing area.
- The surface water content at the Zhurong landing area was estimated by using OMEGA data and then compared with Zhurong data.
- Factors affecting the surface water content inversion model are evaluated and discussed.

Citation: Zhou, X., Liu, Y., Wu, X., Zhao, Z. X., and Zou, Y. L. (2023). Estimation of surface water content at the Tianwen-1 Zhurong landing site. *Earth Planet. Phys.*, *7*(3), 347–355. http://doi.org/10.26464/epp2023035

Abstract: China's first Mars rover, Zhurong, successfully landed in the south of Utopia Planitia. The surface water content at the landing area can provide constraints on mineral formation conditions and help us better understand the evolution of the Martian aqueous and geological environment. In this work, the surface kinetic temperature of the Zhurong landing area was derived by analyzing data from the Mars Express Observatoire pour la Minéralogie, l'Eau, les Glaces et l'Activité (OMEGA) spectrometer. Using the Discrete Ordinate Radiative Transfer (DISORT) model, we performed atmospheric correction and thermal correction for the OMEGA data to obtain the surface effective single-particle absorption thickness (ESPAT) parameter to evaluate the surface water content. The surface water content distribution at the landing area was relatively uniform at a lateral scale of ~10 km. At the Zhurong landing site, the surface water content in the topmost layer (a few hundred micrometers) of the regolith was 5–8 weight percent water (wt% H_2O), assuming surface particle sizes of <45 μm, or 1.6–2.5 wt% H_2O, assuming surface particle sizes in the range of 125–250 μm. The Mars Surface Composition Detector (MarSCoDe) onboard Zhurong also observed significant H_2O/OH signals in the landing area. Our results provide an important regional context for the hydration state of the area and can be further verified by the H content derived from the Laser-Induced Breakdown Spectrometer (LIBS) data of MarSCoDe.

Keywords: Mars; Zhurong; surface water content; Observatoire pour la Minéralogie; l'Eau; les Glaces et l'Activité (OMEGA); Discrete Ordinate Radiative Transfer (DISORT)

1. Introduction

Water plays an important role in planetary evolution and is one of the key parameters for planetary habitability. The data from early telescopes and Image Spectrometer for Mars observed wide absorption in the ~3 μm wavelength range of Martian spectra, which was attributed to aqueous materials on the surface of Mars (Houck et al., 1973; Bibring et al., 1989; Yen et al., 1998; Murchie et al., 2000). In recent years, the Observatoire pour la Minéralogie, l'Eau, les Glaces et l'Activité (OMEGA) onboard the Mars Express and the Compact Reconnaissance Imaging Spectrometer for Mars onboard the Mars Reconnaissance Orbiter have acquired large amounts of Martian visible and near- to mid-infrared spectra, whose absorptions near ~1.4, ~1.9, and ~3.0 μm have been used to identify hydrated minerals (Bibring et al., 2006; Mustard et al., 2008; Liu Y et al., 2012, 2016). Most of the aforementioned water studies are largely qualitative, whereas the surface water content can be further quantified according to the depth of spectral absorption. Initial work attempted to quantify and estimate the surface water content with an apparent absorbance depth near ~3 μm by using the data from Image Spectrometer for Mars (Yen et al., 1998). However, uncertainties of the model were up to ~2 weight percent water (wt% H_2O), and this method did not control for the particle size and albedo of surface materials. The water content inversion parameters of the same material with different particle sizes and albedos are different (Milliken and Mustard, 2005, 2007a, b). Milliken and Mustard (2005) investigated the relationship between water content and various optical parameters at ~1.9 and ~2.9 μm. The absorption at ~2.9 μm was strongly correlated with the absolute water content, whereas the correlation was weaker at ~1.9 μm. Milliken et al. (2007) and Jouglet et al. (2007) performed quantitative spectral analyses of the OMEGA data based on the relationship at ~2.9 μm and

First author: X. Zhou, zhouxiang201@mails.ucas.ac.cn
Correspondence to: Y. Liu, yangliu@nssc.ac.cn
Received 29 DEC 2022; Accepted 25 FEB 2023.
Accepted article online 24 MAR 2023.

derived the water content distribution in some areas of the Martian surface. Their results showed seasonal variations in water content on the Martian surface. The Martian global surface water content assessment by Audouard et al. (2014) showed a slightly different conclusion, however, and in their study, they suggested that the seasonal variation observed previously was probably caused by the effect of water-ice clouds.

Ground-based validation can greatly improve the reliability of the model. For example, the Sample Analysis at Mars instrument onboard Curiosity at the Gale crater (Leshin et al., 2013; Sutter et al., 2017) provided the ground-truth water content (~1–3 wt%) to be used for comparison with the orbital data. Liu Y et al. (2020) used the more advanced Discrete Ordinate Radiative Transfer (DISORT) model to make an atmospheric correction to the OMEGA data and obtained the surface water content at the Gale crater. The surface water content derived from OMEGA data was slightly higher than, but mostly consistent with, the results obtained by Curiosity, which suggests that the method of retrieving the surface water content by using orbital remote sensing data is effective. However, caution should be exercised when using these results.

On May 15, 2021, the Tianwen-1 Zhurong rover successfully landed on Utopia Planitia at 25.066°N, 109.925°E (Liu JJ et al., 2022), providing another excellent opportunity to verify the surface water content inversion method with orbital data. Utopia Planitia is covered with a layer of Hesperian-aged Vastitas Borealis Formation materials (Tanaka and Scott, 1987). These Vastitas Borealis Formation materials have been speculated to be sediment from past flood events (Tanaka et al., 2005) or sublimation residues from an ancient ocean (Kreslavsky and Head, 2002). The landing area is located in the south of the Utopia Planitia, which has a geological age of ~3.34 to 3.68 Ga (Wu X et al., 2021). It contains some layered ejecta craters, giant polygons, and pitted cones (Wu X et al., 2021; Huang H et al., 2023), and these formations have been interpreted to be caused by subsurface water, water ice, or both (Barlow and Perez, 2003; Ivanov et al., 2014; Li L et al., 2015). Liu Y et al. (2022) identified hydrated sulfate or silica minerals at the surface of the landing site based on new data from the Zhurong. The surface water content at the landing area could provide important constraints on the formation mechanism of minerals and help us better understand the evolution of the aqueous and geological environments in Utopia Planitia.

In this work, we used the DISORT model (Stamnes et al., 1988) to perform an atmospheric correction for OMEGA *I*/*F* data (where *I* is radiance and πF is the solar irradiance received at the top of the atmosphere), and we retrieved the surface single scattering albedo (SSA) spectra. By assessing the spectral absorption depth at ~2.9 μm, we estimated the surface water content at the Zhurong landing area. We then discuss the results and the factors that influenced them. Finally, results from our analysis of Zhurong's Short-Wave Infrared Spectrometer (SWIR) and Laser-Induced Breakdown Spectrometer (LIBS) data are given to compare with the orbital observations. The paper is organized as follows. Section 2 introduces the data sets and the processing and inversion methods. Results and discussion of the derived surface water content are presented in Section 3. The conclusions are drawn in Section 4.

2. Data Sets and Methodology

2.1 Data Sets

The OMEGA spectrometer is one of the instruments onboard the Mars Express. It contains 352 spectral elements and can be divided into three channels: the V channel (0.35–1.05 μm), the C channel (1.00–2.77 μm), and the L channel (2.65–5.10 μm). The spectrometer can obtain the reflectance spectra of the topmost layer (about a few hundred micrometers) of the Martian surface (Milliken et al., 2007). The spatial resolution of the instrument is between 300 and 3,000 m, depending on the orbital altitude and detection mode (Bibring et al., 2004). The instrument obtained valid data from 2004 to 2010, covering three Martian years (MY). After 2010, data from the C channel and the L channel were no longer available because of the depletion of coolant. Two OMEGA data sets covering the Zhurong landing site and the surrounding region were selected to retrieve the surface water content. Figure 1 shows the footprint of these two OMEGA data sets. The left swath is orb0973_5, with a spatial resolution of ~0.7 km/pixel, acquired at 15:48 local time in the northern hemisphere summer, covering the Zhurong landing site. The right swath is orb2257_4, with a spatial resolution of ~1.7 km/pixel, acquired at 12:30 local time in the northern hemisphere winter, covering the area close to the Zhurong landing site. The OMEGA data were preprocessed as *I*/*F* from the radiance and were corrected for north–south shift of the L and C channels.

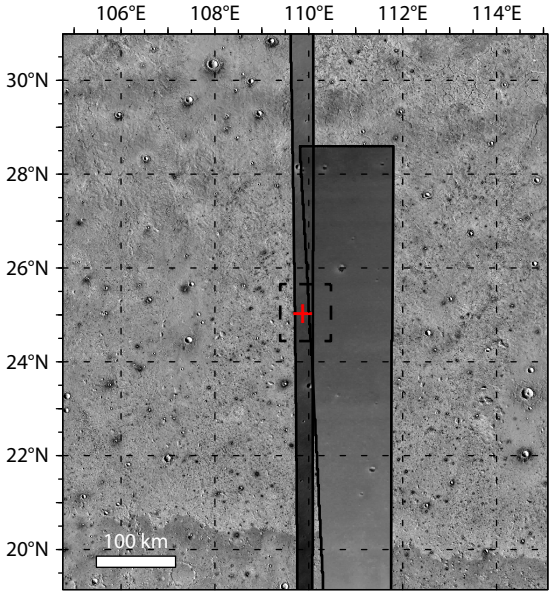

Figure 1. Mosaic map of OMEGA (Observatoire pour la Minéralogie, l'Eau, les Glaces et l'Activité) albedo data at 2.32 μm covering the landing site (red cross symbol) and surrounding area. The swaths on the left and right are orb0973_5 and orb2257_4, respectively, superimposed on the THEMIS (Thermal Emission Imaging System) map. The black dashed box indicates the area shown in Figures 2 and 4.

2.2 Atmospheric Correction

The spectra received by the orbiter are inevitably disturbed by the Martian atmosphere. To obtain the true surface reflectance, it is necessary to remove the contributions of atmospheric gases and aerosols. The traditional atmospheric correction method is an empirical method called the "volcano scan" (e.g., Bibring et al., 2005; Gendrin et al., 2005; Milliken et al., 2007). It removes the contribution of gases in the atmosphere by dividing the orbital spectrum by a scaled standard transmission spectrum. The standard atmospheric spectrum is obtained by dividing the spectrum at the top of Olympus Mons by the spectra at the bottom. The scaled ratio depends on the CO_2 absorption depth at ~2.0 μm. However, the volcano-scan method does not consider the influence of aerosols (such as water ice and dust) and other complex variations of the Martian atmosphere (McGuire et al., 2008).

In this study, we used the DISORT model to remove the contributions of the Martian atmosphere. The DISORT model is based on the first principle and can simulate the transmission of solar radiation through the Martian atmosphere under given observational conditions (Stamnes et al., 1988; Wolff et al., 2009). The physical processes of simulation include the scattering, absorption and thermal emission of gases and aerosols, as well as bidirectional reflection from the surface. Because of the lack of corresponding atmospheric parameters when obtaining the OMEGA data, the temperatures and pressure for each layer of atmosphere and for the aerosol parameters (i.e., ice optical depth and dust optical depth) used in the DISORT model were derived from historical data of the Thermal Emission Spectrometer (TES) at the same longitude, latitude, and solar longitude (Ls; Smith, 2004). More detailed information used in the DISORT model is shown in Table 1. The historical optical depth of ice derived from TES data for orb0973_5 in the Zhurong landing area is as high as 0.09, suggesting that the atmosphere may have a high concentration of water-ice aerosol when the Ls is 104.2°. As described by Audouard et al. (2014), we used the ice cloud index (ICI) proposed by Langevin et al. (2007) to assess the abundance of water-ice clouds, which could be calculated directly from the OMEGA data sets. Madeleine et al. (2012) suggested an ICI value of <0.8 as the threshold for water-ice cloud detection. The ICI value of orb0973_5 was ~0.74, indicating that the water-ice cloud was indeed present when the data were collected. Therefore, the correction for water-ice aerosol was necessary.

Table 1. Information on the OMEGA data parameters used in the DISORT model.[a]

OMEGA data ID	orb0973_5	orb2257_4
Solar longitude	104.2°	307.4°
Subsolar latitude	24.4°N	19.8°S
Incidence angle	52.3°	46.5°
emission angle	0.4°	1.5°
Phase angle	52.4°	45.7°
Surface pressure	7.70 hPa	8.63 hPa
Dust optical depth	0.09	0.20
Ice optical depth	0.09	0.02

[a]OMEGA, Observatoire pour la Minéralogie, l'Eau, les Glaces et l'Activité; DISORT, Discrete Ordinate Radiative Transfer.

The following Hapke functions (Hapke, 2012) were utilized to model surface bidirectional reflection processes:

$$rf(i,e,g)=\frac{\omega}{4}\frac{\mu_0}{\mu_0+\mu}\left\{\left[1+B(g)\right]p(g)+H(\mu_0)H(\mu)-1\right\}S(i,e,g), \quad (1)$$

where *rf* is the radiance factor; *i, e, g* are incidence angles, emission angles, and phase angles, respectively, obtained from the OMEGA observation file; ω is a single-particle scattering albedo, defined as the ratio of scattering efficiency to the sum of absorption efficiency and scattering efficiency; μ_0 and μ are the cos(*i*) and cos(*e*), respectively. The remaining part describes the surface properties, and we used the same parameters as Liu Y et al. (2020). Variable $B(g)$ is a function of the opposition effect, which describes the brightness surge at zero phase angle; $p(g)$ is a phase function describing the single-particle scattering distribution; $H(x)$ describes the multiple scattering; and $S(i, e, g)$ is the shadow function defined by a macroscopic roughness parameter $\bar{\theta}$. The lookup table built from the simulated results could be used to perform the atmospheric correction process.

2.3 Surface Temperature Inversion and Thermal Correction

The surface thermal emission can also influence the orbital spectra. For the OMEGA L channel, the thermal radiation is not negligible (Liu Y et al., 2012). The planet can be approximated as a black body whose thermal radiation is related only to its temperature. Therefore, if the surface temperature of the planet is given, the surface thermal emission can be approximated by Planck's law. Smith (2004) retrieved the Martian global surface temperature between MY24 and MY26 by using infrared spectra from the TES. However, its resolution was too low and was not time sensitive. In this study, we used a method to invert the corresponding surface temperature from OMEGA spectra (Jouglet et al., 2007; Milliken et al., 2007). The spectra near ~5 μm were less influenced by the atmosphere, and the contribution of the Martian surface thermal radiation to the orbital spectrum was relatively significant. Therefore, the orbital spectrum near ~5 μm could be considered to be approximately composed of a solar reflection spectrum and a surface thermal radiation spectrum:

$$I=F\mu_0 R+\epsilon B(T), \quad (2)$$

where *I* is the radiance; *F* is the solar incident irradiance divided by π; μ_0 is the cosine of the incident angle; *R* and ϵ are the reflectance and emissivity of the surface, respectively; and *B* is the thermal emission radiance, which is a function of the surface kinetic temperature *T*. According to Kirchhoff's law, ϵ is supposed to be equal to 1−*R*. If the reflectance is known, then the surface temperature can be retrieved. There is a linear relationship between reflectance at 5 μm and reflectance at 2.5 μm (Jouglet et al., 2007; Milliken et al., 2007), whereas the reflectance at 2.5 μm can be obtained from the OMEGA C channel after atmospheric correction by using DISORT. This method allowed us to acquire the kinetic temperature of each pixel for the OMEGA data, and the total uncertainty of this method was ~4 K (Jouglet et al., 2007). After obtaining the surface temperature, we added the contribution of the Martian surface thermal emission into the DISORT simulation to build a lookup table to derive the surface SSA spectra.

2.4 Surface Water Content Estimation

The bending and stretching vibrations of H_2O, OH, or both produce absorption signatures near ~3 μm (Dyar et al., 2010). The absorption depth of the spectrum can be used to estimate the water content. From the laboratory results of the dehydration of hydrous minerals, Milliken and Mustard (2005, 2007a, b) obtained the relationships between several band parameters and the water content of aqueous minerals. They found an approximately linear relationship between the effective single-particle absorption thickness (ESPAT) parameters at ~2.9 μm and the water weight percentage, which could be expressed as wt% = $A \times$ ESPAT, where A is a parameter related to the mineral composition and particle size. As in previous studies (Audouard et al., 2014, Liu Y et al., 2020), we applied an A of 4.17. It should be noted that an A of 4.17 corresponds to a particle size of < 45 μm (Milliken and Mustard, 2005, 2007a). The ESPAT parameter was defined as the ratio of the absorption efficiency to the scattering efficiency. This parameter relates the relative absorption to the optical path length and can be calculated by SSA ω (Hapke 2012),

$$\mathrm{ESPAT} = \frac{1-\omega}{\omega}. \tag{3}$$

The SSA ω is affected by the apparent spectral intensity and cannot directly reflect the absolute absorption depth of either H_2O or OH. Therefore, the SSA used was continuum removed. Consistent with previous studies, the continuum was defined by the value of the SSA at 2.35 and 3.7 μm because these two spectral bands are almost unaffected by water (Milliken and Mustard, 2007a; Audouard et al., 2014).

3. Results and Discussion

3.1 Surface Temperatures and SSA at the Zhurong Landing Site

The surface kinetic temperatures were derived from the OMEGA data and are shown in Figure 2. Figure 2a shows the mosaic temperature map for the swath of orb0973_5, which was obtained in the Martian northern hemisphere summer. The temperature range of the region was between 247 and 253 K at the local time of ~15:48. Figure 2b shows the mosaic temperature map of orb2257_4 at the time of the northern hemisphere winter.

We obtained the SSA spectrum based on the retrieved temperature map and the DISORT model. Figure 3a shows the uncorrected I/F spectra obtained by OMEGA. The spectra had significant atmospheric contamination, such as CO_2 absorption at ~1.6, ~2.0, and ~2.6 μm and water-ice aerosol absorption at ~1.5 μm. At wavelengths of >2.5 μm, thermal emission from the Martian surface also increased the intensity of reflectance detected by the OMEGA instrument. Figure 3b shows the SSA spectra after DISORT atmospheric and thermal corrections. The red line is the spectrum at the landing site in Figure 2a, and the blue line is the spectrum closest to the landing site in Figure 2b. The spectrum at the landing site shows a strong water absorption feature at ~3.0 μm, suggesting that the surface water content near the landing site may be relatively high.

3.2 Surface Water Content at the Zhurong Landing Site

From the derived SSA spectra and using the method described in Section 2.4, we evaluated the surface water content of the area within 1° × 1° covering the landing site (Figure 4). In summer, the surface water content of the area around the landing site at the topmost layer (about a few hundred micrometers) of the Martian regolith was ~7–8 wt%, with an uncertainty of 0.5–1 wt%. The discrepancy of the surface water content in the overlap area between the summer and winter data sets was ~0.5 wt%. Previous work by Audouard et al. (2014) showed that seasonal variation of the water weight percentage at 25°N was ~1 wt%. Thus, considering the uncertainty of our method, the seasonal variation of the surficial water content at the landing area was not obvious, consistent with the results of Audouard et al. (2014).

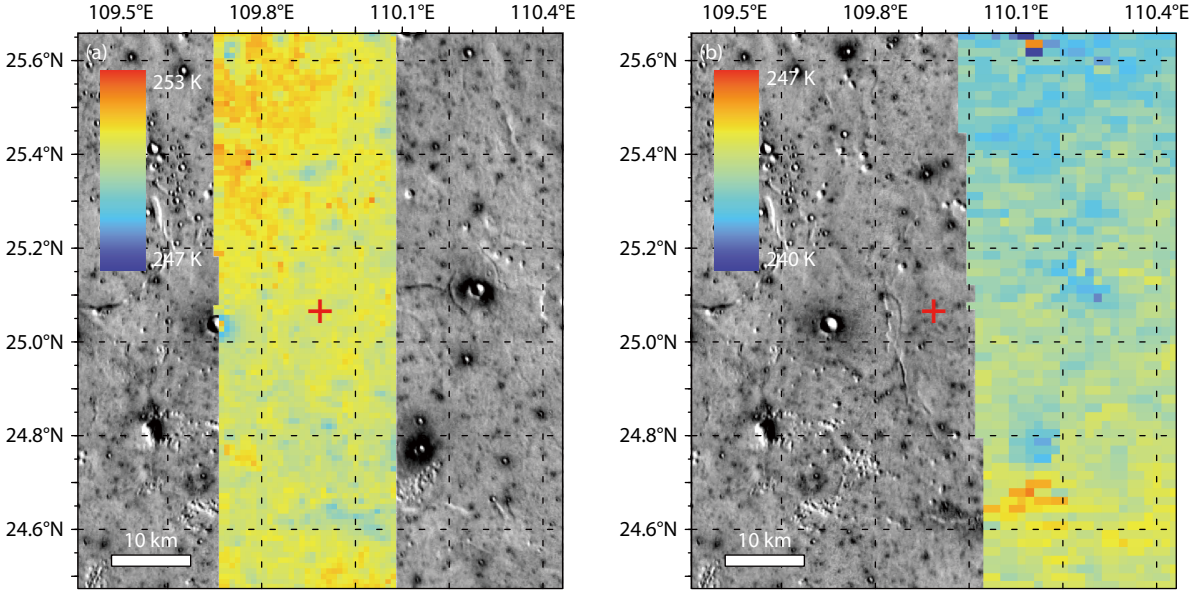

Figure 2. Zoomed mosaic map of the surface kinetic temperature covering the Zhurong landing area. The Zhurong landing site is denoted by a red cross. (a) The temperature corresponding to orb0973_5. (b) The temperature corresponding to orb2257_4.

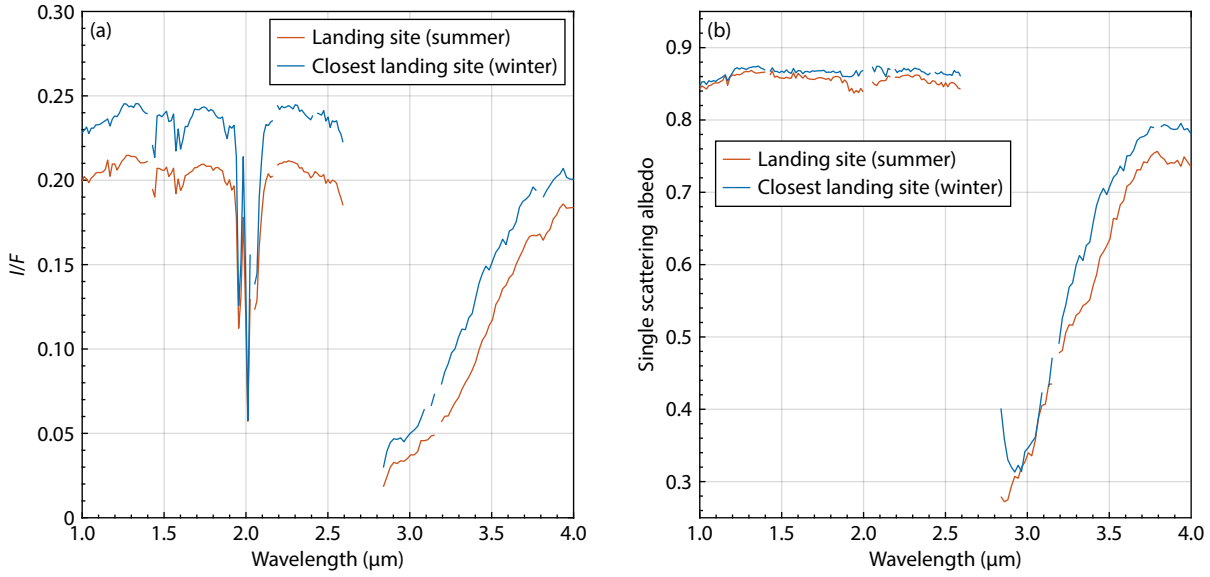

Figure 3. The *I/F* (radiance/solar irradiance at the top of the atmosphere divided by π) spectra extracted from OMEGA (Observatoire pour la Minéralogie, l'Eau, les Glaces et l'Activité) data sets (a) and the derived single scattering albedos (b). The spectrum at the landing site is depicted in red, whereas the spectrum near the landing site is depicted in blue. The bad bands have been removed.

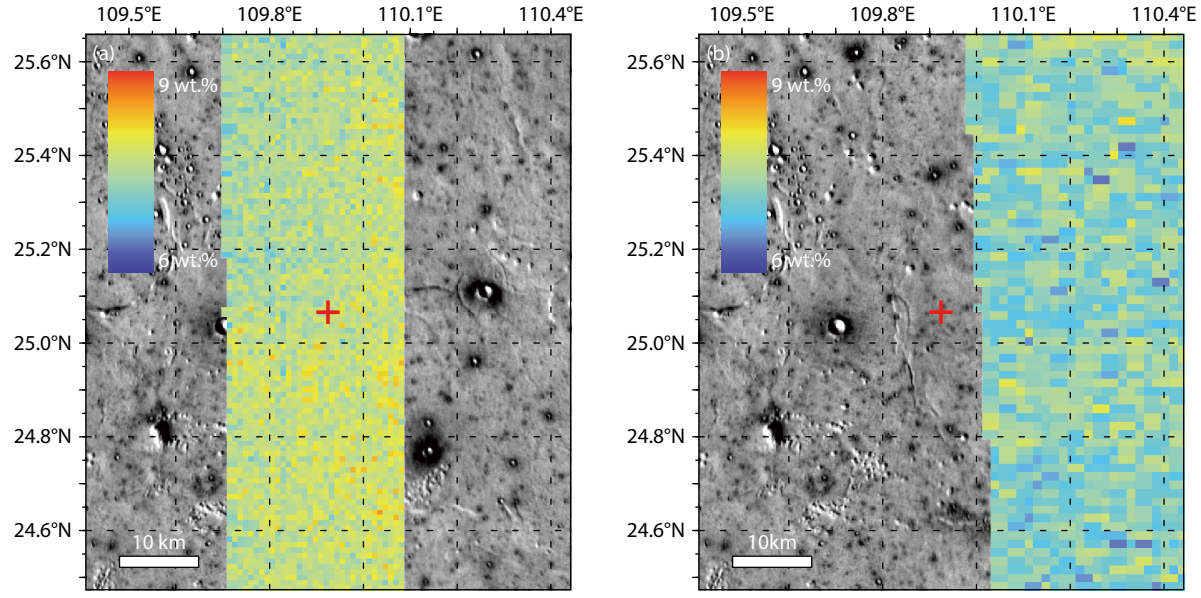

Figure 4. Map of the surface water content distribution over the Zhurong landing site and surrounding area. (a) Retrieved results from the summer swath orb0973_5. (b) Retrieved results from the winter swath orb2257_4.

Compared with the volcano-scan method, the DISORT model considers the correction for aerosols. If the relevant parameters used in the DISORT simulation are accurate, then using DISORT for atmospheric correction should be more accurate than using the empirical volcano-scan method (McGuire et al., 2008). Atmospheric correction by the DISORT model is sensitive to the atmospheric parameters; however, it is difficult to obtain the corresponding real atmospheric parameters when acquiring the OMEGA data. The ice and dust optical depth parameters used in our model are historical data derived from TES data at the same latitude, longitude, and Ls (Smith, 2004). This will bring some uncertainty to the inversion results. The influence of the dust aerosol optical depth parameter used in the DISORT model on the derived surface water content was discussed by Liu Y et al. (2020), who found that the derived surface water content was higher when using a higher optical depth of the dust aerosol. In this work, we derived the surface water content of the Zhurong landing site under different water ice optical depths. Figure 5a shows the derived surface water content when using different water ice optical depths at the Zhurong landing site for the OMEGA observation of orb0973_5. As the optical depth value of water-ice aerosol used in the model increased, the derived water content of the surface decreased. This was because the higher optical depth value meant that more water-ice aerosols were removed from the model, leading to a lower derived surface water content. We used the ICI value (Langevin et al., 2007) to evaluate the relative abundance of water-

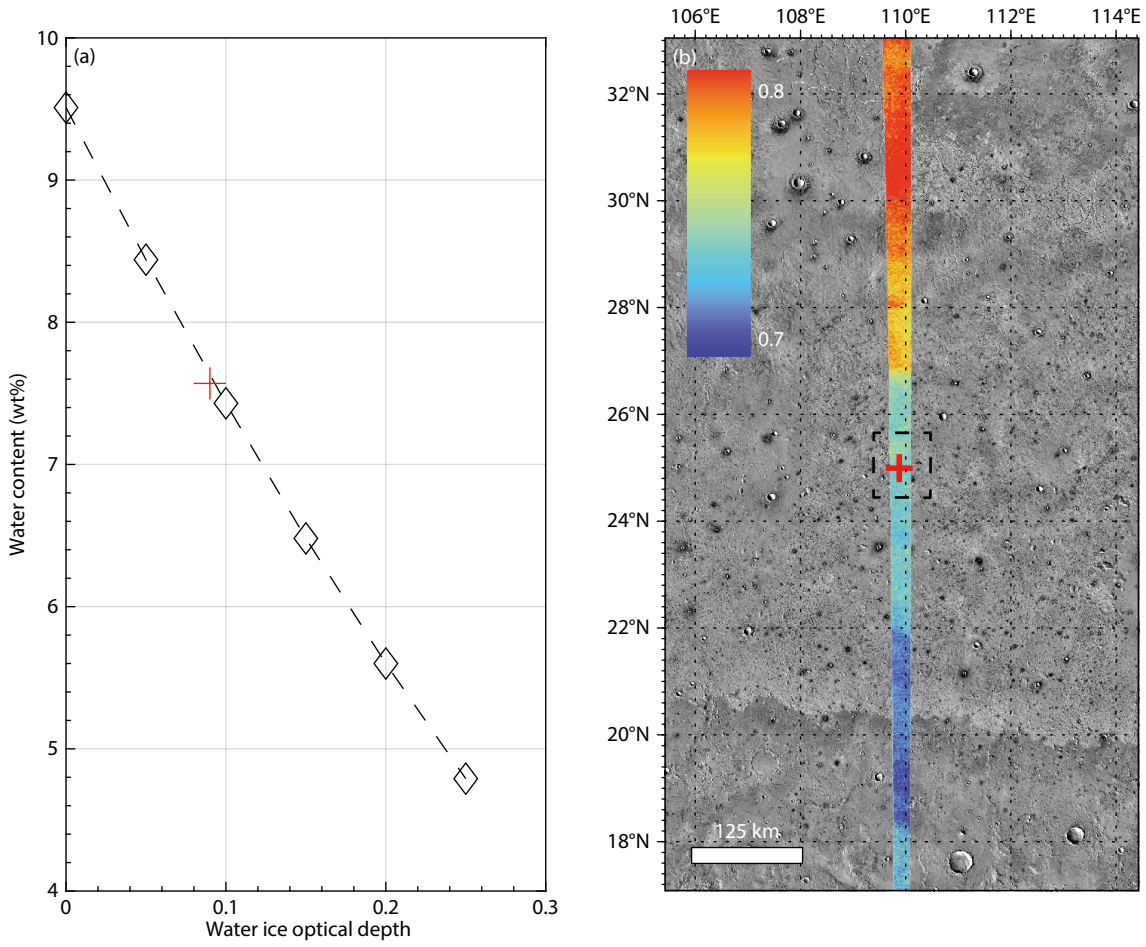

Figure 5. (a) Surface water content derived under different water ice optical depth parameters at the Zhurong landing site. (b) Map of the ice cloud index value derived from orb0973_5.

ice aerosols, and these results are shown in Figure 5b. It can be observed that a lower value of ICI on the map means a higher abundance of water-ice aerosols. In the same swath, the region covered the most by water-ice clouds was determined by the ICI value to be located from 18°N to 22°N. The Zhurong landing site had moderate ICI values, and the corresponding surface water content was approximately 7.5 wt%. The discrepancies between historical and actual optical depths can cause uncertainty in the derived surface water content.

For the same OMEGA data sets used in this study, we also performed a surface water content inversion by using the volcano-scan atmospheric correction method (Milliken et al., 2007). Except for use of the atmospheric correction method, the rest of the processing was the same as described in Section 2. For the summer swath, the derived surface water content using the volcano-scan method was ~1.2 wt% lower than the result derived from the DISORT method. For the winter swath, the derived surface water content from the volcano-scan method was ~2 wt% lower than the result derived from the DISORT method. Theoretically, the DISORT model, which is based on the first principle, is more accurate than the empirical volcano-scan model (McGuire et al., 2008). However, it is presently difficult to assess the accuracy of the atmospheric parameters used by the DISORT model, and the quality of OMEGA data decreased in the later stages of the instrument. Considering these factors, we cannot determine which atmospheric correction method gave more accurate results. Therefore, we estimate that the surface water content at the Zhurong landing site is 5–8 wt%. Verification of the surface water content will be performed by the measurement of H abundance with LIBS on the Zhurong Mars rover in future work.

In addition, the surface water content derived from ESPAT spectra strongly relies on particle size (Milliken and Mustard, 2007b). We used the assumption that the surface particle size was <45 μm and the linear parameter *A* was 4.17 (Milliken et al., 2007; Audouard et al., 2014; Liu Y et al., 2020). Minitti et al. (2013) visually assessed the particle size of the interior Rocknest sand shadow by using the Mars Hand Lens Imager onboard Curiosity. They found that 0.5- to 2-mm-diameter particles constituted <10%, 100- to 150-μm-diameter particles constituted between 40% and 60%, and finer particles constituted between 30% and 50%. Therefore, the Martian surface particle size distribution is more complex than previously thought, and the assumption of particles <45 μm may not be suitable. If the particle size is assumed to be 125–250 μm, corresponding to a linear parameter *A* of 1.30 (Milliken et al., 2007), the derived surface water content is 3.2 times smaller and the surface water content at the Zhurong landing site becomes 1.6–2.5 wt%, which is closer to the surface water content obtained from previous landing missions (Biemann et al., 1977;

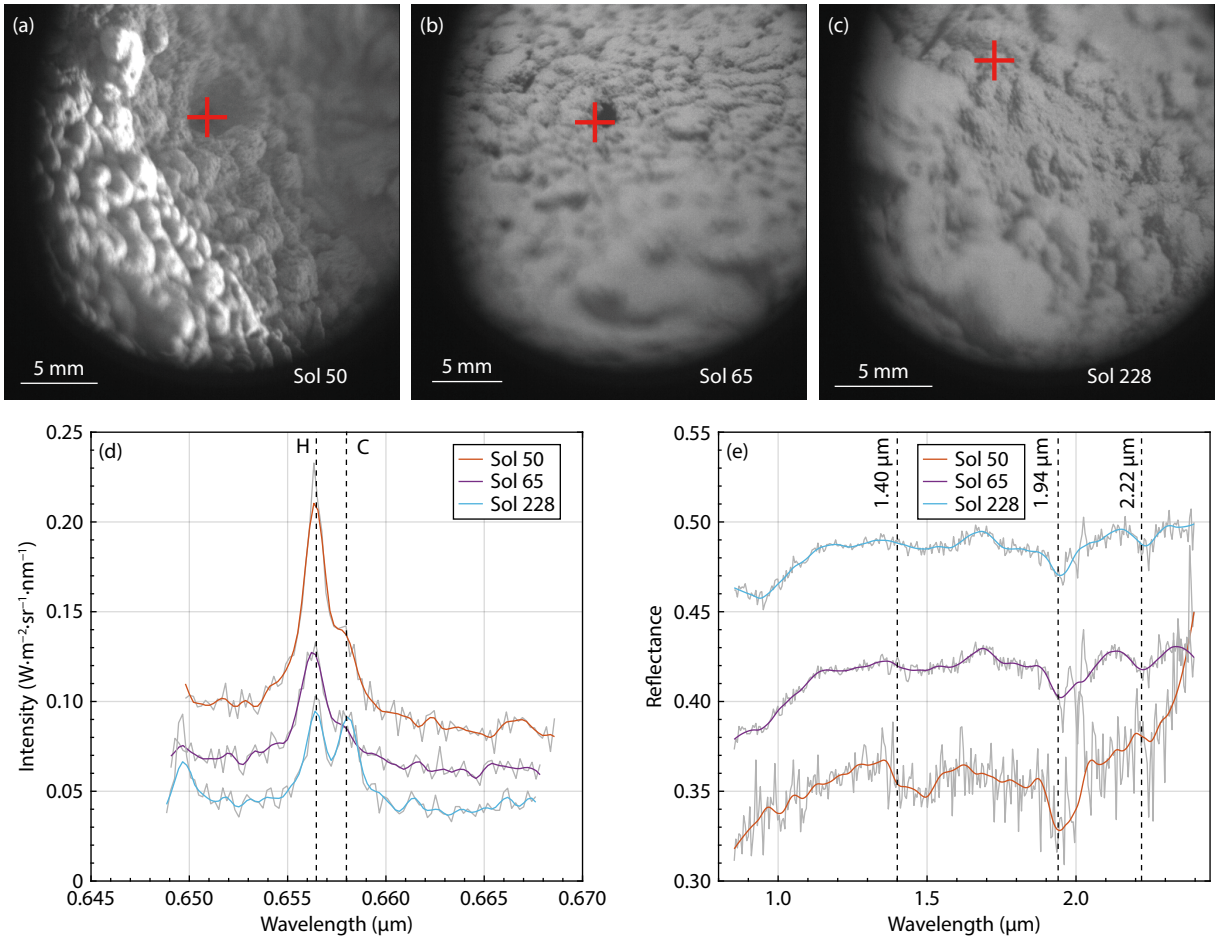

Figure 6. *In situ* observations of the Mars Surface Composition Detector onboard the Zhurong rover. (a, b, c) Micro-images of the surface material. The red cross denotes the Laser-Induced Breakdown Spectrometer (LIBS) and Short-Wave Infrared Spectrometer (SWIR) observation point. (d) LIBS spectra of the surface material. The dotted lines are emission of the H element (656.46 nm) and the C element (657.99 nm). (e) SWIR spectra of the surface material. The dotted lines are located at 1.40, 1.94, and 2.22 μm. The smoothed spectra (colored lines) overlay the raw spectra (gray line).

Anderson and Tice, 1979; Leshin et al., 2013; Sutter et al., 2017). It is worth noting that the microscopic images of the surface of the landing site taken by the Micro-Imaging Camera onboard the Zhurong rover show plenty of coarse grains (Figure 6a–c), indicating that the surface water content at the Zhurong landing site may be overestimated with the orbital data because of the assumed finer grain size.

3.3 *In situ* Observations

The *in situ* observations by the Zhurong rover found evidence for hydrated sulfate or silica minerals at the landing site (Liu Y et al., 2022), suggesting that the water activity was more active in Utopia Planitia during the Amazonian than previously thought. The MarSCoDe (consisting of the Micro-Imaging Camera, LIBS, and SWIR) onboard the Zhurong rover obtained batches of data at the landing site and along the traverse path. Here, we extracted three representative LIBS spectra to examine the peaks indicative of the presence of H in the regolith. These representative LIBS spectra came from three coarse-grained targets along the traverse path (Figure 6a–c), with a particle size of >1 mm in diameter. In all three spectra analyzed, we found a strong H emission signal (656.46 nm) in the LIBS data of Zhurong (Figure 6d), suggesting abundant presence of the H element.

The SWIR spectra at the same detection point also showed an obvious H_2O/OH absorption characteristic, including the band absorptions at ~1.9 μm (combination modes of molecular H_2O) and ~2.2 μm (OH stretches; Dyar et al., 2010). These obvious H signals and H_2O/OH absorption characteristics indicate that the Zhurong landing area may have a high surface water content. In addition to having the strongest H signal in the LIBS spectrum, the coarse grains of Sol 50 also have a structural OH absorption characteristic at ~1.4 μm (first O-H stretch overtone; Dyar et al., 2010). Aside from the surface adsorbed water, the structural water may be an important component of the coarse grains. The coarse-grained material may play a more important role in orbital remote sensing detection than previously thought.

4. Conclusions

We estimated the surface water content at the Zhurong landing area by ESPAT at ~2.9 μm from OMEGA data. Considering the uncertainties of the atmospheric correction method and the surface water content inversion model, the upper layer of the regolith at the Zhurong landing site was estimated to be ~5–

8 wt%, assuming surface particle sizes of <45 μm, or ~1.6–2.5 wt%, assuming surface particle sizes in the range of 125–250 μm. The distribution of surface water content at the Zhurong landing area was relatively uniform at the kilometer scale, and the surface of the landing area had no significant seasonal variation in water content. Our results provide essential constraints on the evolution of the water environment in this area. Both LIBS and SWIR data from the Zhurong rover captured significant H_2O/OH signals of coarse grains in the landing area, suggesting that coarse grains may play a more important role in water detection from the orbital remote sensing data than previously thought. In the future, the surface water content analyzed from LIBS can be further compared with the orbital inversion results to provide a basis for the reliability test and correction of the surface water content inversion model when using the orbital data.

Acknowledgments

Portions of the data sets used in this work are available from the Mars Orbital Data Explorer at Washington University in St. Louis, Missouri, USA (http://ode.rsl.wustl.edu/mars/), and the Lunar and Planetary Data Release System (https://moon.bao.ac.cn/web/enmanager/home). Portions of the scientific data were provided by the China National Space Administration. We are very grateful for the excellent work of the Mars Express OMEGA team and the Tianwen-1 team. This work was funded by the National Key Research and Development Project (Grant No. 2019YFE0123300), the National Natural Science Foundation of China (Grant No. 42072337), and the preresearch project on Civil Aerospace Technologies (Grant Nos. D020101 and D020102) funded by the China National Space Administration through the Pandeng Program of the National Space Science Center, Chinese Academy of Sciences, Key Research Program of the Chinese Academy of Sciences (Grant No. ZDBS-SSW-TLC001).

References

Anderson, D., and Tice, A. (1979). The analysis of water in the Martian regolith. *Journal of Molecular Evolution*, *14*, 33–38.

Audouard, J., Poulet, F., Vincendon, M., Milliken, R. E., Jouglet, D., Bibring, J. P., Gondet, B., and Langevin, Y. (2014). Water in the Martian regolith from OMEGA/Mars Express. *J. Geophys. Res.*: *Planets*, *119*(8), 1969–1989. https://doi.org/10.1002/2014je004649

Barlow, N. G., and Perez, C. B. (2003). Martian impact crater ejecta morphologies as indicators of the distribution of subsurface volatiles. *J. Geophys. Res.*: *Planets*, *108*(E8), 5085. https://doi.org/10.1029/2002JE002036

Bibring, J. P., Combes, M., Langevin, Y., Soufflot, A., Cara, C., Drossart, P., Encrenaz, T., Erard, S., Forni, O., … Sotin, C. (1989). Results from the ISM experiment. *Nature*, *341*(6243), 591–593. https://doi.org/10.1038/341591a0

Bibring, J. P., Soufflot, A., Berthé, M., Langevin, Y., Gondet, B., Drossart, P., Bouyé, M., Combes, M., Puget, P., … Forget, F. (2004). OMEGA: Observatoire pour la Minéralogie, l'Eau, les Glaces et l'Activité, in Mars Express: The Scientific Payload, edited by A. Wilson, Eur. Space Agency Spec. Publ., ESA SP-1240, 37–49.

Bibring, J. P., Langevin, Y., Gendrin, A., Gondet, B., Poulet, F., Berthé, M., Soufflot, A., Arvidson, R., Mangold, N., … The OMEGA team. (2005). Mars surface diversity as revealed by the OMEGA/Mars Express observations. *Science*, *307*(5715), 1576–1581. https://doi.org/10.1126/science.1108806

Bibring, J. P., Langevin, Y., Mustard, J. F., Poulet, F., Arvidson, R., Gendrin, A., Gondet, B., Mangold, N., Pinet, P., … Neukum, G. (2006). Global mineralogical and aqueous Mars history derived from OMEGA/Mars Express data. *Science*, *312*(5772), 400–404. https://doi.org/10.1126/science.1122659

Biemann, K., Oro, J., Toulmin III, P., Orgel, L., Nier, A., Anderson, D., Simmonds, P., Flory, D., Diaz, A., and Rushneck, D. (1977). The search for organic substances and inorganic volatile compounds in the surface of Mars. *Journal of Geophysical Research*, *82*(28), 4641–4658. https://doi.org/10.1029/JS082i028p04641

Dyar, M., Hibbitts, C., and Orlando, T. (2010). Mechanisms for incorporation of hydrogen in and on terrestrial planetary surfaces. *Icarus*, *208*(1), 425–437. https://doi.org/10.1016/j.icarus.2010.02.014

Gendrin, A., Mangold, N., Bibring, J. P., Langevin, Y., Gondet, B., Poulet, F., Bonello, G., Quantin, C., Mustard, J., … Lemouélic, S. (2005). Sulfates in Martian layered terrains: The OMEGA/Mars Express view. *Science*, *307*(5715), 1587–1591. https://doi.org/10.1126/science.1109087

Hapke, B. (2012). *Theory of Reflectance and Emittance Spectroscopy* (2nd ed). Cambridge: Cambridge University Press.

Houck, J. R., Pollack, J. B., Sagan, C., Schaack, D., and Decker, J. A., Jr. (1973). High altitude infrared spectroscopic evidence for bound water on Mars. *Icarus*, *18*(3), 470–480. https://doi.org/10.1016/0019-1035(73)90156-5

Huang, H., Wang, X., Chen, Y., Zhang, Q., Zhao, F. Y., Ren, X., Zeng, X. G., Yan, W., Chen, W. L., ... Liu, J. J. (2023). Observations and interpretations of geomorphologic features in the Tianwen-1 landing area on Mars by using orbital imagery data. *Earth Planet. Phys.*, *7*(3), 331–346. https://doi.org/10.26464/epp2023005

Ivanov, M. A., Hiesinger, H., Erkeling, G., and Reiss, D. (2014). Mud volcanism and morphology of impact craters in Utopia Planitia on Mars: Evidence for the ancient ocean. *Icarus*, *228*, 121–140. https://doi.org/10.1016/j.icarus.2013.09.018

Jouglet, D., Poulet, F., Milliken, R. E., Mustard, J. F., Bibring, J. P., Langevin, Y., Gondet, B., and Gomez, C. (2007). Hydration state of the Martian surface as seen by Mars Express OMEGA: 1. Analysis of the 3 μm hydration feature. *J. Geophys. Res.*: *Planets*, *112*(E8), E08S06. https://doi.org/10.1029/2006je002846

Kreslavsky, M. A., and Head, J. W. (2002). Fate of outflow channel effluents in the northern lowlands of Mars: The Vastitas Borealis Formation as a sublimation residue from frozen ponded bodies of water. *J. Geophys. Res.*: *Planets*, *107*(E12), 5121. https://doi.org/10.1029/2001JE001831

Langevin, Y., Bibring, J. P., Montmessin, F., Forget, F., Vincendon, M., Douté, S., Poulet, F., and Gondet, B. (2007). Observations of the south seasonal cap of Mars during recession in 2004–2006 by the OMEGA visible/near-infrared imaging spectrometer on board Mars Express. *J. Geophys. Res.*: *Planets*, *112*(E8), E08S12. https://doi.org/10.1029/2006je002841

Leshin, L. A., Mahaffy, P. R., Webster, C. R., Cabane, M., Coll, P., Conrad, P. G., Archer, P. D. Jr., Atreya, S. K., Brunner, A. E., … Moores, J. E. (2013). Volatile, isotope, and organic analysis of martian fines with the Mars Curiosity rover. *Science*, *341*(6153), 1238937. https://doi.org/10.1126/science.1238937

Li, L., Yue, Z. Y., Di, K. C., and Peng, M. (2015). Observations of Martian layered ejecta craters and constraints on their formation mechanisms. *Meteorit. Planet. Sci.*, *50*(3), 508–522. https://doi.org/10.1111/maps.12438

Liu, J. J., Li, C. L., Zhang, R. Q., Rao, W., Cui, X. F., Geng, Y., Jia, Y., Huang, H., Ren, X., … Zhang, H. B. (2022). Geomorphic contexts and science focus of the Zhurong landing site on Mars. *Nat. Astron.*, *6*(1), 65–71. https://doi.org/10.1038/s41550-021-01519-5

Liu, Y., Arvidson, R. E., Wolff, M. J., Mellon, M. T., Catalano, J. G., Wang, A. L., and Bishop, J. L. (2012). Lambert albedo retrieval and analyses over Aram Chaos from OMEGA hyperspectral imaging data. *J. Geophys. Res.*: *Planets*, *117*(E11), E00J11. https://doi.org/10.1029/2012je004056

Liu, Y., Glotch, T. D., Scudder, N. A., Kraner, M. L., Condus, T., Arvidson, R. E., Guinness, E. A., Wolff, M. J., and Smith, M. D. (2016). End-member identification and spectral mixture analysis of CRISM hyperspectral data: A case study on southwest Melas Chasma, Mars. *J. Geophys. Res.*: *Planets*, *121*(10), 2004–2036. https://doi.org/10.1002/2016je005028

Liu, Y., Stachurski, F., Liu, Z. H., and Zou, Y. L. (2020). Quantitative assessment of water content and mineral abundances at Gale crater on Mars with orbital observations. *Astron. Astrophys.*, *637*, A79. https://doi.org/10.1051/0004-6361/201937045

Liu, Y., Wu, X., Zhao, Y. Y. S., Pan, L., Wang, C., Liu, J., Zhao, Z. X., Zhou, X., Zhang,

C. L., … Zou Y L. (2022). Zhurong reveals recent aqueous activities in Utopia Planitia, Mars. *Sci. Adv.*, *8*(19), eabn8555. https://doi.org/10.1126/sciadv.abn8555

Madeleine, J. B., Forget, F., Spiga, A., Wolff, M. J., Montmessin, F., Vincendon, M., Jouglet, D., Gondet, B., Bibring, J. P., … Schmitt, B. (2012). Aphelion water-ice cloud mapping and property retrieval using the OMEGA imaging spectrometer onboard Mars Express. *J. Geophys. Res.*: *Planets*, *117*(E11), E00J07. https://doi.org/10.1029/2011je003940

McGuire, P. C., Wolff, M. J., Smith, M. D., Arvidson, R. E., Murchie, S. L., Clancy, R. T., Roush, T. L., Cull, S. C., Lichtenberg, K. A., … Malaret, E. R. (2008). MRO/CRISM retrieval of surface Lambert albedos for multispectral mapping of Mars with DISORT-based radiative transfer modeling: Phase 1—Using historical climatology for temperatures, aerosol optical depths, and atmospheric pressures. *IEEE Trans. Geosci. Remote Sens.*, *46*(12), 4020–4040. https://doi.org/10.1109/TGRS.2008.2000631

Milliken, R., and Mustard, J. (2007a). Estimating the water content of hydrated minerals using reflectance spectroscopy I. Effects of darkening agents and low-albedo materials. *Icarus*, *189*(2), 550–573. https://doi.org/10.1016/j.icarus.2007.02.017

Milliken, R., and Mustard, J. (2007b). Estimating the water content of hydrated minerals using reflectance spectroscopy: II. Effects of particle size. *Icarus*, *189*(2), 574–588. https://doi.org/10.1016/j.icarus.2006.12.028

Milliken, R. E., and Mustard, J. F. (2005). Quantifying absolute water content of minerals using near-infrared reflectance spectroscopy. *J. Geophys. Res.*: *Planets*, *110*(E12), E12001. https://doi.org/10.1029/2005je002534

Milliken, R. E., Mustard, J. F., Poulet, F., Jouglet, D., Bibring, J. P., Gondet, B., and Langevin, Y. (2007). Hydration state of the Martian surface as seen by Mars Express OMEGA: 2. H_2O content of the surface. *J. Geophys. Res.*: *Planets*, *112*(E8), E08S07. https://doi.org/10.1029/2006je002853

Minitti, M. E., Kah, L. C., Yingst, R. A., Edgett, K. S., Anderson, R. C., Beegle, L. W., Carsten, J. L., Deen, R. G., Goetz, W., … van Beek, T. (2013). MAHLI at the Rocknest sand shadow: Science and science-enabling activities. *J. Geophys. Res.*: *Planets*, *118*(11), 2338–2360. https://doi.org/10.1002/2013JE004426

Murchie, S., Kirkland, L., Erard, S., Mustard, J., and Robinson, M. J. I. (2000). Near-infrared spectral variations of Martian surface materials from ISM imaging spectrometer data. *Icarus*, *147*(2), 444–471. https://doi.org/10.1006/icar.2000.6446

Mustard, J. F., Murchie, S. L., Pelkey, S. M., Ehlmann, B. L., Milliken, R. E., Grant, J. A., Bibring, J. P., Poulet, F., Bishop, J., … Wolff, M. (2008). Hydrated silicate minerals on Mars observed by the Mars Reconnaissance Orbiter CRISM instrument. *Nature*, *454*(7202), 305–309. https://doi.org/10.1038/nature07097

Smith, M. D. (2004). Interannual variability in TES atmospheric observations of Mars during 1999–2003. *Icarus*, *167*(1), 148–165. https://doi.org/10.1016/j.icarus.2003.09.010

Stamnes, K., Tsay, S. C., Wiscombe, W., and Jayaweera, K. (1988). Numerically stable algorithm for discrete-ordinate-method radiative transfer in multiple scattering and emitting layered media. *Appl. Opt.*, *27*(12), 2502–2509. https://doi.org/10.1364/AO.27.002502

Sutter, B., McAdam, A. C., Mahaffy, P. R., Ming, D. W., Edgett, K. S., Rampe, E. B., Eigenbrode, J. L., Franz, H. B., Freissinet, C., … Yen, A. S. (2017). Evolved gas analyses of sedimentary rocks and eolian sediment in Gale Crater, Mars: Results of the Curiosity rover's sample analysis at Mars instrument from Yellowknife Bay to the Namib Dune. *J. Geophys. Res.*: *Planets*, *122*(12), 2574–2609. https://doi.org/10.1002/2016JE005225

Tanaka, K. L., and Scott, D. H. (1987). Geologic map of the polar regions of Mars. U.S. Geological Survey, Geologic Investigations Series Map I-1802-C.

Tanaka, K. L., Skinner, J. A., Jr., and Hare, T. M. (2005). Geologic map of the northern plains of Mars. U.S. Geological Survey.

Wolff, M. J., Smith, M. D., Clancy, R. T., Arvidson, R., Kahre, M., Seelos, F., Murchie, S., and Savijärvi, H. (2009). Wavelength dependence of dust aerosol single scattering albedo as observed by the Compact Reconnaissance Imaging Spectrometer. *J. Geophys. Res.*: *Planets*, *114*(E2), E00D04. https://doi.org/10.1029/2009je003350

Wu, X., Liu, Y., Zhang, C. L., Wu, Y. C., Zhang, F., Du, J., Liu, Z. H., Xing, Y., Xu, R., … Zou, Y. L. (2021). Geological characteristics of China's Tianwen-1 landing site at Utopia Planitia, Mars. *Icarus*, *370*, 114657. https://doi.org/10.1016/j.icarus.2021.114657

Yen, A. S., Murray, B. C., and Rossman, G. R. (1998). Water content of the Martian soil: Laboratory simulations of reflectance spectra. *J. Geophys. Res.*: *Planets*, *103*(E5), 11125–11133. https://doi.org/10.1029/98JE00739